Picosecond time-resolved spectroscopy of a controlled preformed plasma heated by an intense subpicosecond laser pulse

C. Y. Côté,[1,*] J. C. Kieffer,[1] and O. Peyrusse[2]
[1]*Institut National de la Recherche Scientifique—Énergie et Matériaux, Université du Québec, Québec, Canada, J3X 152*
[2]*Commissariat à l'Energie Atomique, Centre de Limeil-Valenton, 94195 Villeneuve St.-Georges, France*
(Received 31 October 1996; revised manuscript received 11 February 1997)

The experimental work presented in this paper focuses on the consequences of both nonlocal heat transport and rapid time variation in atomic physics as a function of the initial gradient scale length of a plasma. We look at the time history of *K*-shell emission when an intense 0.53-μm high-contrast pulse heats aluminum plasmas having a chosen gradient scale length. We compare our experimental results to hydrodynamics and atomic physics calculations and we study three different plasma regimes. When the laser pulse interacts with an ultrashort density gradient scale length, the plasma is at local thermodynamic equilibrium and the calculations are in very good agreement with the experimental results. These calculations also agree with the observed spectra in the case of a long gradient scale length (nonstationary Maxwellian regime). However, in the intermediate regime, the observed time history of the Li-like satellite lines is strongly affected by transient atomic physics and nonlocal thermal transport. In this particular regime, the calculated spectra are strongly dependent on the thermal transport model used in the simulations. Simulations in the intermediate regime can therefore be benchmarked and tested against our experimental spectra. [S1063-651X(97)03207-8]

PACS number(s): 52.25.Nr, 52.50.Jm, 52.65.−y, 52.70.La

I. INTRODUCTION

The recent advent of compact high-intensity subpicosecond lasers gives access to new regimes of laser-matter interaction [1–3]. In particular, the interaction of ultrashort laser pulses with solid target is a technique used by several groups to create high-energy-density matter and to generate bright x-ray sources [4–10]. These plasmas produced and heated by ultrashort laser pulses are characterized by highly transient and nonequilibrium states resulting from the very short temporal and spatial scales involved [6,11,12]. Furthermore, the characteristic gradient scale length of these short plasmas can be smaller than the electron mean free path and thus nonlocal treatment of heat transport is necessary [13].

Much progress has been made in the understanding of atomic physics and x-ray generation in solid density plasmas produced by subpicosecond pulses. However, only a few experimental works address the issue of nonlocal transport in such plasmas. In a previous work [14], we used the polarization of x-ray line emission to evaluate the second-order anisotropy of the electron velocity distribution related to nonlocal electron heat flow. These experiments were realized with a short pulse superimposed to a long and low-intensity pedestal. This pedestal could not be controlled independently of the main short pulse. Nonlocal heat transport was observed, but could not be studied as a function of the preformed plasma gradient scale length. Furthermore, these measurements were integrated in time. Recently, calculations [13] indicated that non-Maxwellian and nonstationary effects strongly modify line intensity ratios and in particular the Li-like spectrum was greatly changed. The experimental work presented in this paper focuses on the consequences of both nonlocal heat transport and rapid time variation in atomic physics as a function of the initial gradient scale length of the plasma. More specifically, we look at the time history of *K*-shell emission produced by aluminum ions near 1.6 keV. Because the atomic structure of aluminum is quite well known, this material is very convenient for experiments and results can be easily used to benchmark numerical calculations.

Here we present and discuss time-resolved spectra obtained (with a 1.5-ps temporal resolution) when an intense 0.53-μm-high contrast pulse heats a controlled gradient scale length plasma. In these experiments, we isolate and analyze three different plasma regimes: the local thermal equilibrium (LTE) regime, the transient nonlocal regime, and the transient Maxwellian regime. Results obtained in those three regimes are presented and compared. Picosecond time-resolved spectra that we have previously presented were obtained at low intensity (10^{16} W/cm^2) for plasmas produced by a 1-μm, 500-fs pulse (with a pedestal) [4,15] and by a high-contrast (pedestal-free) 0.53-μm 400-fs pulse [16]. More recently, we measured time-resolved keV [17] and sub-keV [18] spectra for the case of a very-high-contrast 0.53-μm pulse interacting with solid targets at 10^{18} W/cm^2. The time history of electron density was inferred on the picosecond time scale. A few other groups working with subpicosecond lasers also reported time-resolved spectra in the keV [19,20] and soft-x-ray (sub-keV) range [21].

In this work, the experimental conditions are chosen to avoid complex laser-plasma interaction processes such as profile steepening, resonance absorption, and parametric instabilities. The measured fraction of laser energy in hot electrons is negligible here, even for large gradient scale lengths, in contrast to what is measured at larger intensity [22].

In Sec. II. we describe the modeling of plasma evolution

*Present address: Center for Ultrafast Optical Science, University of Michigan, Ann Arbor, MI 48109-2099.

and of the interaction of a short pulse with a preformed plasma. The experimental techniques and sample of raw data are shown in Sec. III. Results, theoretical fits, and a discussion are presented in Sec. IV (LTE plasma) and in Sec. V (transient nonlocal and transient Maxwellian plasmas). Conclusions and suggestions for future work are presented in Sec. VI.

II. INTERACTION OF A SHORT PULSE WITH A PREFORMED PLASMA

The experiments presented here were realized with two collinear 500-fs pulses, normally incident on a target at modest intensity (10^{16} W/cm^2) and separated by a variable time delay. The delay between the two pulses allowed us to adjust the gradient scale length (L) seen by the second pulse. In these conditions, even when L is large, nonlinear processes (resonance absorption and parametric instabilities) are not important and the hot-electron population is negligible.

These interaction conditions are modeled with a one-fluid, two-temperature Eulerian code that solves the equations of hydrodynamics in planar geometry [23]. It includes a wave equation solver [1,3] to model self-consistently the laser energy deposition as well as the ponderomotive force. The model also integrates a non-steady-state atomic physics package based on the quasi-steady-state approximation [24,25] to model ionization and recombination. We simultaneously solve the equations of continuity for the mass density, the momentum equation of the fluid, the equations for the ionic and electronic energy, and the n_z+1 rate equations governing the evolution of ground-state ionic fraction. The population of the excited levels of a given ionic species is assumed to instantaneously follow the populations of the two adjacent ground states. Laser energy deposition is determined by solving the Helmoltz equation [1,3] along with hydrodynamics. The electron-ion collision frequency is calculated using Spitzer's [26] formula and then corrected to take the laser field into account (Schlessinger-Wright correction) [27] and kinetic effects (Langdon correction) [28]. We used the formulation proposed recently by Vick *et al.* [29] to couple those two corrections. The electron thermal conduction is treated either with a flux-limited conduction model [30] or with the nonlocal Epperlein-Short model [31]. In the flux-limited model, the Fourier's heat flux formulation is artificially limited to a maximum value corresponding to a fraction (f) of the free streaming heat flux [30,32]. The value of the flux limiter (f) is usually chosen to recover thermal penetration observed experimentally. In both the flux-limited and Epperlein-Short models, we corrected the Spitzer-Harm electron thermal conductivity in order to recover the solid heat conductivity in the low-temperature high-density limit [33].

The x-ray spectrum emitted in a given spectral range is predicted by running our multicell time-dependent atomic model (TRANSPEC [34]) from the density, temperature, and velocity profiles calculated at regular time intervals in the hydrodynamics simulation. TRANSPEC includes radiative transfer between cells. The laser pulses are modeled as spatially uniform over the focal spot, with a Gaussian temporal profile [450 fs at full width at half maximum (FWHM)] that represent a good fit to autocorrelation traces.

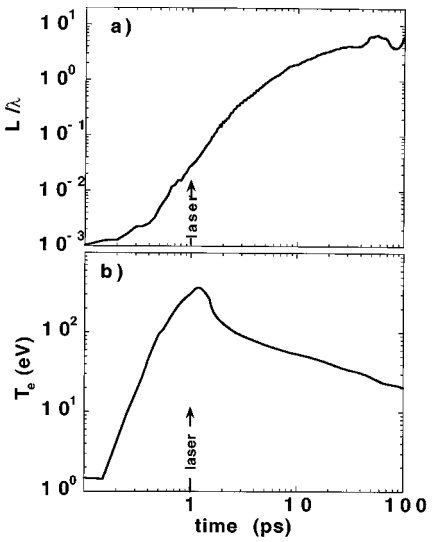

FIG. 1. Time history of the plasma parameters calculated at a critical density ($n_e=4\times10^{21}$ cm^{-3}). A Gaussian pulse ($\lambda=0.5$ μm and 450 fs FWHM) is normally incident at 10^{16} W/cm^2 on a steep density gradient scale length ($L/\lambda=10^{-3}$). The arrows indicate the time of maximum laser intensity.

Figure 1 shows the time history of some plasma parameters [gradient scale length in Fig. 1(a) and electron temperature in Fig. 1(b)] at a critical density ($n_e=4\times10^{21}$ cm^{-3}) predicted by the hydrodynamics calculations for a plasma produced by a 0.53-μm, 450-fs FWHM pulse focused at 10^{16} W/cm^2 on a solid aluminum target. After the laser pulse has interacted with the target, the plasma undergoes an adiabatic expansion and a cold plasma with large gradient scale length can be achieved after a few tens of picoseconds. Figure 2 presents the time history of the plasma parameters calculated at the critical density for an irradiation at 10^{16} W/cm^2 (0.53-μm, 450-fs FWHM pulse) of an aluminum plasma formed 40 ps earlier by an identical pulse. More precisely, we look at the variation of the local gradient scale length (L), electron and ion temperatures (T_e and T_i, respectively), and ionization (Z^*). Just before the arrival of the second pulse the plasma parameters are $L/\lambda=5$ (where λ is the laser wavelength), $T_e-T_i\sim30$ eV, and $Z^*=5$. Then the electron temperature increases very quickly and an ion-

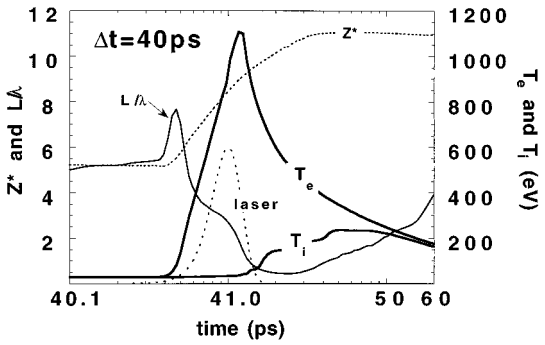

FIG. 2. Time history of plasma parameters calculated at a critical density ($n_e=4\times10^{21}$ cm^{-3}). A 0.5-μm, 450-fs FWHM laser pulse is normally incident at 10^{16} W/cm^2 on an aluminum plasma preformed 40 ps earlier by an identical pulse. Thermal transport is treated in the flux-limited mode with $f=0.15$.

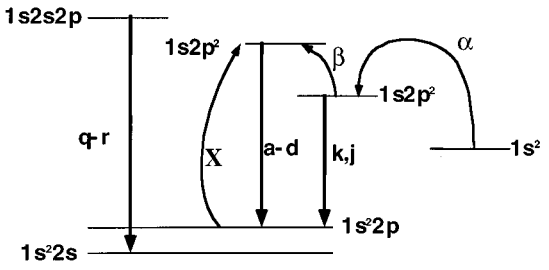

FIG. 3. Simplified schematic of energy levels corresponding to Li-like satellites of the aluminum He_α line.

ization front proceeds through the conduction zone producing a steepening of the electron density profile. At the peak of the second pulse, we have $L/\lambda = 2.7$ and $T_e = 950$ eV. At that time, 7% of the laser energy is absorbed by the plasma. Similar behavior, with some slight variations, is observed at other delays.

Here we study in particular the Li-like spectrum $[1s2l2l'(l,l'=0,1)\text{-}1s^2 2l(l=0,1)]$. Some of the chief lines are schematically represented in Fig. 3 using Gabriel's notation [35]. The upper level of the k,j transition ($ls2p^2$) is mainly populated by dielectronic recombination from a He-like ion [36], the rate of which is represented by α. For the $a-d$ transition, the upper level mainly depends on the collisional excitation rate (X) from the first excited state $ls^2 2p$ and from collisional mixing (β) between both upper levels. When the density becomes close to the solid density, this collisional mixing imposes a Boltzmann equilibrium among all upper levels of Li-like satellite lines [37]. In these conditions, collisional broadening is important due to electron impacts and the $a-d$ to k,j intensity ratio is close to its LTE value of 1 [34]. These features have also been observed in our previous experiments with 0.53-μm irradiation [38]. When the laser pulse interacts with a longer density gradient scale length, emission is produced at lower density. Line broadening is weaker and collisional mixing (β) between both upper levels becomes less important. In this regime, the $a-d$ to k,j intensity ratio depends on the ratio of the Li- and He-like populations and can therefore be used to probe nonstationary effects on atomic physics [11,12] occurring when the plasma is heated on a time scale that is short compared to the ionization and excitation characteristic times. Moreover, when nonlocal transport causes the electron velocity distribution to deviate from a Maxwellian distribution, this ratio can be strongly enhanced due to an increase of the collisional excitation rate (noted X in Fig. 3) from the first excited state $1s^2 2p$ [13]. In the case of very long gradient scale lengths, nonlocal effects become negligible and nonstationary effects dominate the Li-like spectrum. Therefore, by controlling the delay between the two pulses and by monitoring the Li-like emission, we should be able to observe the transition from a LTE plasma regime (for $L/\lambda \ll 1$) to a thermal nonlocal plasma regime (intermediate L values) and then to a thermal nonstationary Maxwellian plasma regime ($L/\lambda \gg 1$).

III. EXPERIMENT

These experiments were carried out with the Table Top Terawatt laser system at the Institut National de la Recherche Scientifique. A 550-fs, 1.053-μm laser pulse with an energy up to 1 J was provided by a Nd:glass system based on the chirped-pulse amplification technique [39] and including a fiber-optics pulse cleaner [40]. The infrared pulse was frequency doubled using a potassium dihydrogen phosphate type-I crystal with a conversion efficiency of 50%. Near-solid-density plasmas were generated by focusing a single high-contrast (10^{10}:1) green pulse at an intensity of 10^{16} W/cm^2 at normal incidence on solid targets using a spherical $f/6$ fused silica lens. The interaction with a plasma having longer gradient scale length was achieved using two pulses with an adjustable time delay between them (0–200 ps). This was realized using a Michelson interferometer to generate two collinear 0.53-μm pulses that were focused with an $f/6$ spherical fused silica lens on a thick solid target (50-μm focal spot) giving intensity of 10^{16} W/cm^2 for each pulse. Here we essentially used low intensities to avoid nonlinear processes and thus to benchmark the computer simulations. The interaction of a 0.53-μm pulse at higher intensity with a preformed plasma has been studied [41] in a different experiment by focusing the unconverted 1-μm radiation at 10^{16} W/cm^2 using an $f/6$ lens to generate a 100-μm-diam plasma having a controlled gradient scale length, while the green pulse (p polarized) was focused at 45° incidence angle onto a 10-μm spot (5×10^{17} W/cm^2) by means of an off-axis parabola ($f/3$). This regime exhibits strong nonlinear processes and a large fraction of laser energy in hot electrons and large ponderomotive effects have been observed.

Time-resolved spectra were obtained with a streak camera coupled to a Von-Hamos crystal spectrometer [42]. The temporal resolution of the whole detection system was 1.5 ps and its spectral resolution was 5 mÅ at 8 Å. This allowed us to study temporal behavior of Li-like emission [17]. Figure 4 shows time-resolved spectra obtained when the laser pulse interacts with a plasma generated by an identical pulse 40 and 100 ps earlier. We can see that in both cases Be-like emission is produced first and that x-ray line duration increases with the ionization state. Since ionization states produced at low or intermediate temperature will exist only during the rise time of the laser pulse, the Be-like emission is expected to be observed before Li- and He-like emissions.

For a delay of 20 ps between the creation of the plasma and the arrival of the second pulse, the Be-like and Li-like emission peaks are observed, respectively, 2.5 and 1.5 ps before the maximum of He-like emission (Fig. 5). It is important to note that temporal resolution is 1.5 ps and that the given values for the delay between Be-, Li-, and He-like emission with $\Delta t = 20$ ps are averaged from a statistic analysis of about ten measurements. In the following, we mainly compare time-resolved Li-like spectra to computer simulations for different time delay between both laser pulses.

IV. NEAR-SOLID-DENSITY PLASMAS

At very high electron density, the high collisional rates almost establishes Boltzmann equilibrium between the upper levels of Li-like satellite lines, the energy difference between the doubly excited levels being small compared to the electron temperature. In a previous paper [43], we analyzed a higher-intensity regime in which the radiation pressure balances the thermal pressure, maintaining a very steep density

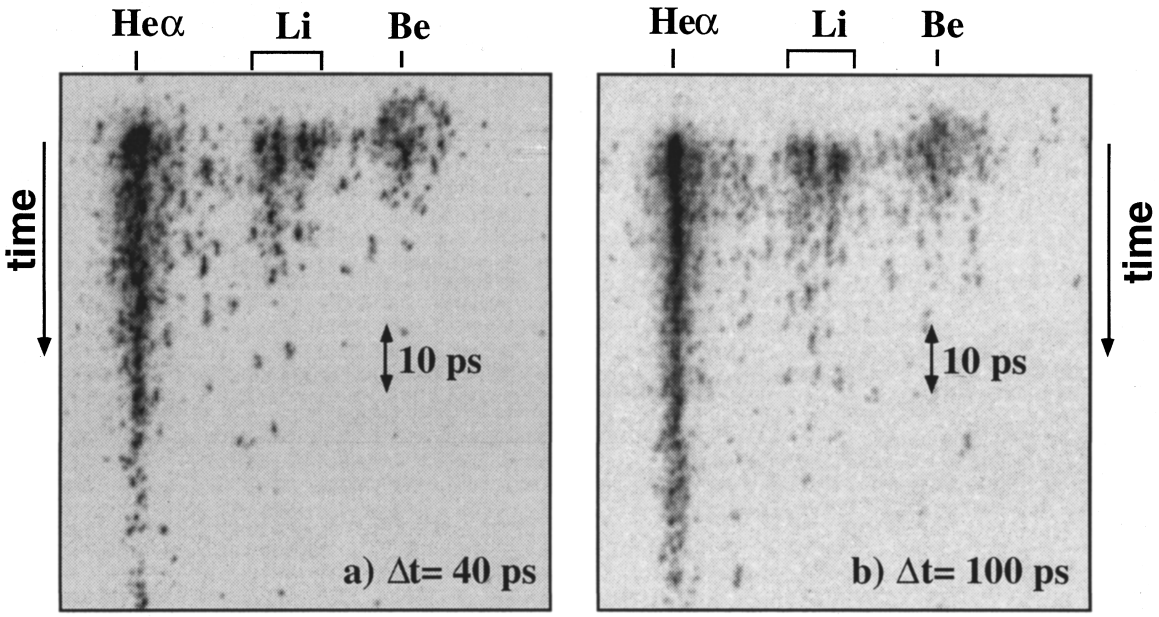

FIG. 4. Time-resolved experimental spectrum produced by the interaction of a 10^{16}-W/cm^2 laser pulse focused at normal incidence on a plasma produced earlier by an identical pulse. The time delay between both laser pulses is (a) 40 ps and (b) 100 ps.

gradient during the energy deposition and thus forcing the emission to be produced in a region where density is close to solid density. In this work, a near-solid-density regime was achieved during the interaction of the high-contrast pulse focused at 10^{16} W/cm^2 on the solid aluminum target. The time-integrated spectrum recorded near the resonant He-like line appears in Fig. 6. The solid line is the calculated time-integrated spectrum (numerical integration of the computed time-dependent spectrum), which has been normalized to the peak of the measured He_α line for comparison. The $1s2lnl'$ satellites with $n>2$ located on the red side of the He_α line are not included in these calculations. We note that the data and the calculated spectrum are in satisfactory agreement. In Fig. 7 the measured time history of the He_α line is compared to calculations. The result obtained from the codes shows a duration that is shorter than the measurements, even when the calculation is convoluted with the measured camera line spread function to take the limited temporal resolution into account. Despite this difference, it is gratifying to note the very good agreement between the measured He_γ time-integrated line profile (sensitive to both the electron density and the ion temperature through the ion microfield) and the calculated integrated profile (Fig. 8).

The time-integrated Li-like spectra obtained in the same experimental conditions exhibits a significant line broadening mainly caused by electron impacts. The ratio of $a-d$ lines (upper levels, mostly core excited) on k,j lines (upper levels populated by dielectronic capture) is close to the LTE value. Figure 9 shows that the spectrum fits well with a LTE calculation at an electron temperature of 250 eV and an electron density of about 10^{23} cm^{-3} (the aluminum Li-like solid electron density is 6×10^{23} cm^{-3}).

Thus these comparisons at 10^{16} W/cm^2 indicate that the calculations can be used with some good level of confidence as a guideline for the interpretation of the results as a function of the gradient scale length. For this LTE regime the

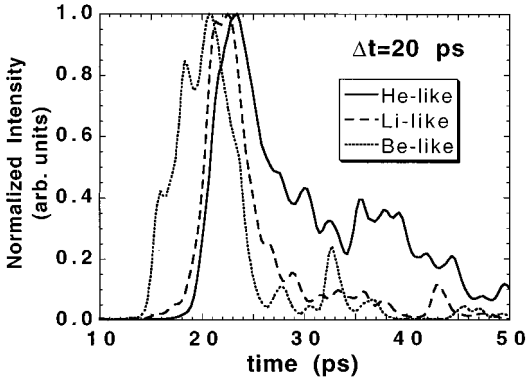

FIG. 5. Time history of line emission corresponding to various ionization states. The delay between both laser pulses is 20 ps. The Be-like emission is assumed to be generated during the peak intensity of the second laser pulse and the emission intensities have been normalized for clarity.

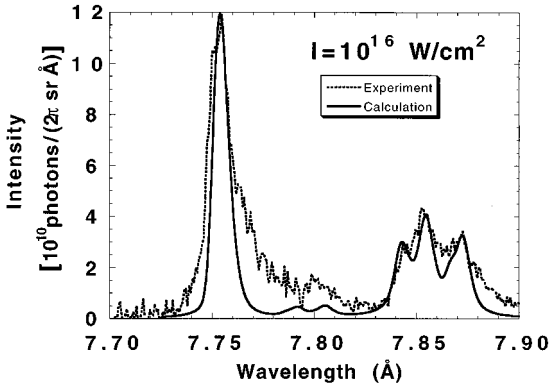

FIG. 6. Time-integrated spectrum of aluminum recorded near the He_α line. The dotted line is the experimental result and the full line represents the spectrum calculated with the hydrodynamics code coupled to TRANSPEC. The error bar on wavelength calibration is 2 mÅ.

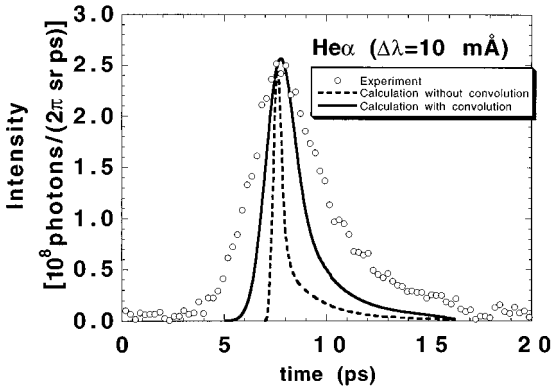

FIG. 7. Time history of the He_α line. The dots represent the experimental result and the dotted line is the time history calculated with the hydrodynamics code coupled to TRANSPEC. This calculation was convoluted with a 1.5-ps FWHM Gaussian to take the instrumental resolution into account (full line). The error bar on time calibration is 1.5 ps, which corresponds to the resolution of the camera.

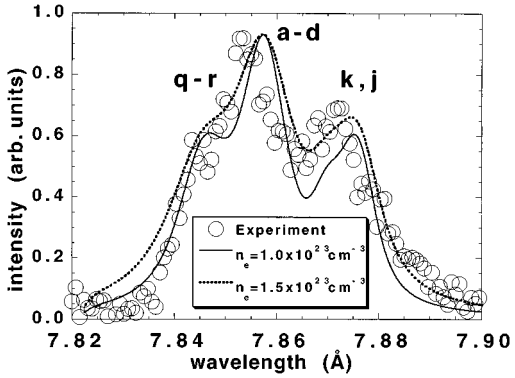

FIG. 9. Time-integrated profile of aluminum Li-like satellite lines. The experimental profile (dots) is compared to the profiles calculated with TRANSPEC in the LTE mode for an electron temperature of 250 eV and different electron densities. The best fit is obtained with a density of 10^{23} cm^{-3}. The experimental error bar on wavelength calibration is 2 mÅ.

calculations indicate that the He-like and Li-like emissions are mainly produced at, respectively, $n_e=5\times10^{22}$ cm^{-3}, $T_e=280$ eV, and $T_i=75$ eV and $n_e=10^{23}$ cm^{-3}, $T_e=250$ eV, and $T_i=75$ eV.

V. NONEQUILIBRIUM PLASMAS

When the clean short laser pulse interacts with an extremely short density gradient scale length, the Li-like emission is mostly produced at large density and the $a-d$ to k,j line intensity ratio has a value close to the LTE value, as previously discussed. However, when the pulse interacts with a longer gradient scale length plasma, emission is produced at lower electron density (less than 10^{23} cm^{-3}). The $a-d$ to k,j intensity ratio can be enhanced due to transient and non-Maxwellian effects that increase, respectively, the population of Li-like ions compared to the He-like population and the collisional excitation rate from the first excited state $1s^22p$ (represented by X in Fig. 3). Such an enhancement is observed (Fig. 10) for the cases of intermediate delay (around 10 ps) between both laser pulses. The open dots in Fig. 10 represent the data obtained from time integrated Li-like spectra. The time-integrated value for the one pulse irradiation (2ω alone) is close to 1, which corresponds to the LTE value. The dotted and solid lines are the result of a time-dependent calculation with a flux limiter of, respectively, $f=0.15$ and $f=0.07$ for thermal conduction. Calculations with the Epperlein-Short delocalization model give results similar to the one obtained with $f=0.15$. For very short and very long delays corresponding, respectively, to short ($L/\lambda<10^{-1}$) and long ($L/\lambda>3$) gradient scale lengths, the result is independent of the flux limiter f and we observe good agreement between calculations and experiments. Small values of the flux limiter ($f=0.07$) are necessary to recover the behavior of the $a-d$ to k,j ratio observed for $L/\lambda\sim1$. This figure emphasizes two key features of this intermediate regime. First, the delocalization model (which implicitly assumes a stationary heat flux) fails to represent the experiment. Second, the quantitative understanding of this regime crucially depends on the way thermal transport is treated. Although the agreement obtained by severely limiting the thermal flux is interesting, this adjustable f parameter

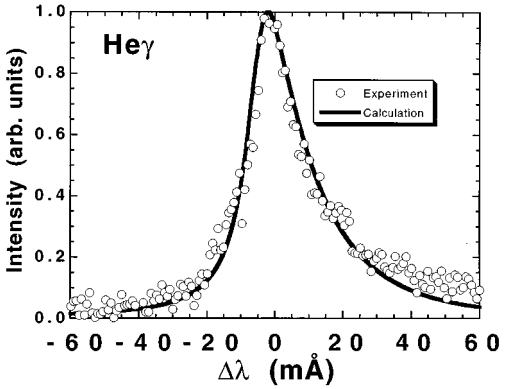

FIG. 8. Time-integrated profile of the aluminum He_γ line. The experimental profile (dots) is compared to the profile calculated with the hydrodynamics code coupled to TRANSPEC. The error bar on wavelength calibration is 2 mÅ.

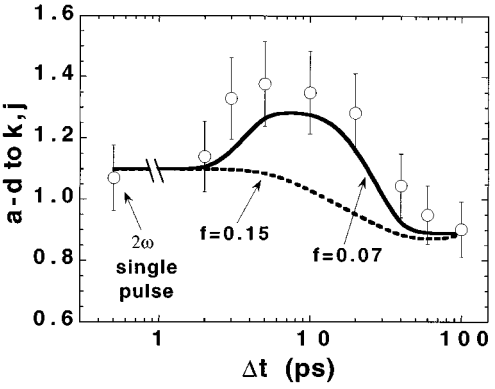

FIG. 10. Ratio of time-integrated Li-like satellites $a-d$ to k,j as a function of the delay (Δt) between both laser pulses. The experimental values are represented by the open dots. The hydrodynamics calculation was done using a flux limiter of $f=0.07$ (full line) and $f=0.15$ (dotted line).

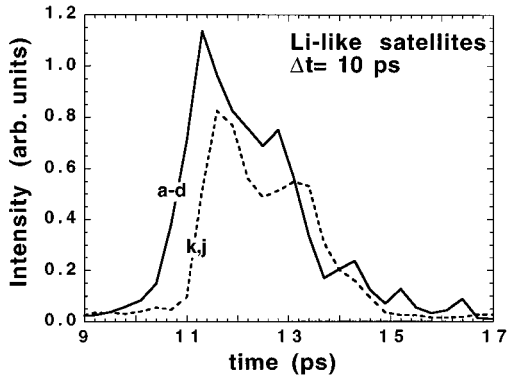

FIG. 11. Time history of Li-like $a-d$ and k,j satellite lines obtained during the interaction of a 10^{16}-W/cm^2 laser pulse with an aluminum plasma created 10 ps earlier by a similar pulse.

is a trick and in this intermediate regime the nonlocal character of the heat transport cannot be neglected [13]. In these experimental conditions, a kinetic simulation [44] was performed using the FPI code [45] and TRANSPEC [34]. As usual, the Eulerian hydrodynamics code was used to simulate the first 10 ps of the plasma expansion. Then the plasma parameters were taken as initial conditions for FPI and the results were post-processed with TRANSPEC. The resulting Li-like spectrum presents a ratio of $a-d$ to $k,j=1.45$, which is very close to the value observed experimentally for $\Delta t=10$ ps (Fig. 10). For very long gradient scale length (which corresponds to long delays) nonlocal effects are negligible since the experimental $a-d$ to k,j time-integrated ratio is recovered using the nonstationary model only. In the following, we discuss time-resolved spectra obtained for a 10-ps delay (identified as the transient nonlocal regime) and for a 100-ps delay (identified as the transient Maxwellian regime).

A. Transient nonlocal regime

Figure 11 presents the time history of $a-d$ and k,j Li-like satellite lines obtained with two collinear pulses separated by 10 ps. As observed with the time-integrated results (Fig. 10), the flux limiter (f) has a strong influence on the calculated time history of satellite lines shown in Fig. 12. The $a-d$ lines are enhanced and k,j emission is slightly delayed with smaller f [Fig. 12(a)]. In these calculations the laser peaks at 11 ps and dielectronic recombination emission is delayed by 1 ps. It is interesting at this point to compare experimental and calculated time-resolved Li-like spectra. Figure 13 presents this comparison at the time 11.5 ps (slightly after the $a-d$ line maximum) and at a later time ($t=13.5$ ps). At the earlier time, the higher flux limiter ($f=0.15$) result fails to represent the intensity of both $a-d$ and $q-r$ line groups [Fig. 13(a)]. The calculation with $f=0.07$ represents the experimental spectrum relatively well, but some differences still persist for the k,j lines [Fig. 13(b)]. At a later time, which corresponds to the expanding and recombining plasma, the calculated spectral shape does not depend on the flux limiter (f) and represent fairly well the observed spectrum [Fig. 13(c)]. Both the nonlocal and nonstationary effects are present in this regime and produce the observed behavior. The calculation adequately reproduces the general behavior of the time evolution of $a-d$ to k,j but it slightly

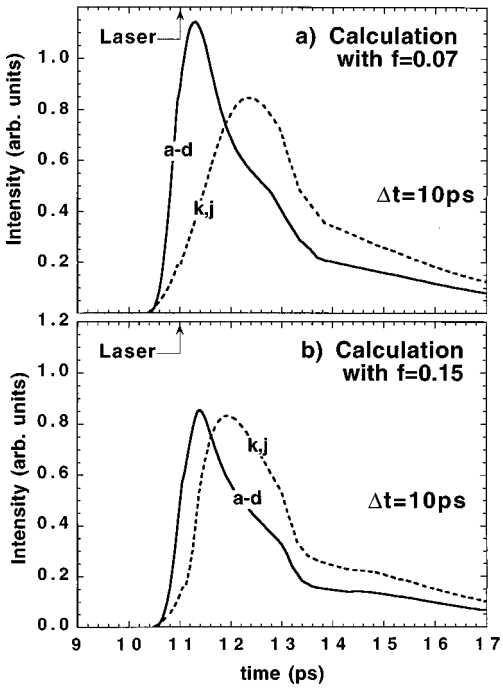

FIG. 12. Calculated time history of Li-like $a-d$ and k,j satellite lines obtained during the interaction of a 10^{16}-W/cm^2 laser pulse with an aluminum plasma created 10 ps earlier by a similar pulse. The value of the flux limiter is (a) $f=0.07$ and (b) $f=0.15$.

underestimates the maximum value (Fig. 14) because non-Maxwellian effects are not taken into account. Indeed, the kinetic simulation (FPI plus TRANSPEC) gives a maximum ratio of about 6, which corresponds to the experimental value. The hydrodynamics code indicates that the emission is produced near a critical density and the Fokker-Planck calculations show that in this region, the electron distribution is not very far from a Maxwellian distribution [44]. However, in this particular regime, a kinetic treatment of thermal transport is still necessary to calibrate the flux limiter of a fluid code in order to recover Li-like line ratio observed experimentally.

B. Transient Maxwellian regime

Figure 15 presents the time history of the $a-d$ and k,j Li-like lines obtained with the two collinear pulses separated by 100 ps. For a large L/λ, non-Maxwellian effects related to nonlocal transport are weak and do not affect the Li-like satellites [13]. However, we can see that the collisional core-excited $a-d$ lines are still produced before the k,j lines. The observed time history of the $a-d$ to k,j line intensity ratio (Fig. 16) is in good agreement with a time-dependent calculation (independently of the flux limiter). This result also reveals transient effects (here observed as an ionization delay) that enhance the inner-shell excited satellites ($a-d$) due to a delayed appearance of He-like ions limiting dielectronic capture on the upper levels of the k,j transitions. In these conditions, the actual calculations reproduce the He_α time history in a satisfactory way (Fig. 17).

C. He_γ line shape

We previously noted the very good agreement between the measured He_γ time-integrated line profile and the calcu-

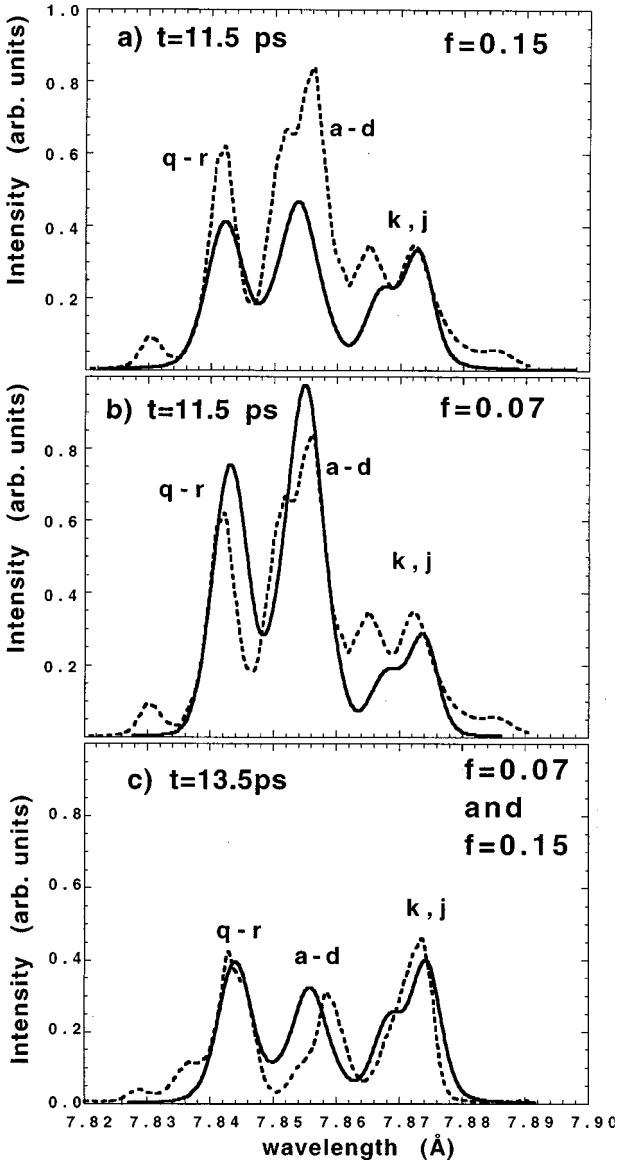

FIG. 13. Instantaneous Li-like spectra observed at different times. At $t=11.5$ ps, the spectrum is compared to calculations obtained with a flux limiter of (a) $f=0.15$ and (b) $f=0.07$. At a later time, (c) $t=13.5$, the calculation is independent of the flux limiter.

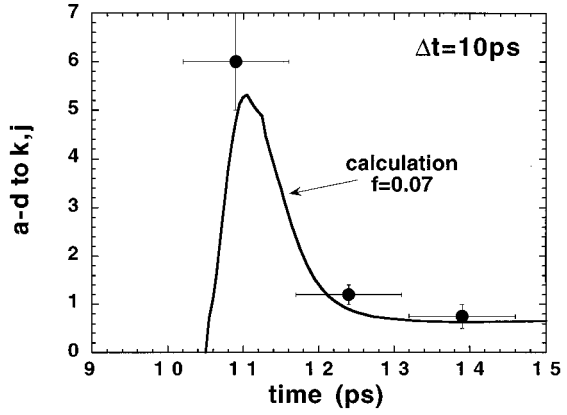

FIG. 14. Measured time history of Li-like $a-d$ to k,j ratio (dots) and comparison with calculation (line) obtained with a flux limiter of $f=0.07$. The delay between both laser pulses is 10 ps.

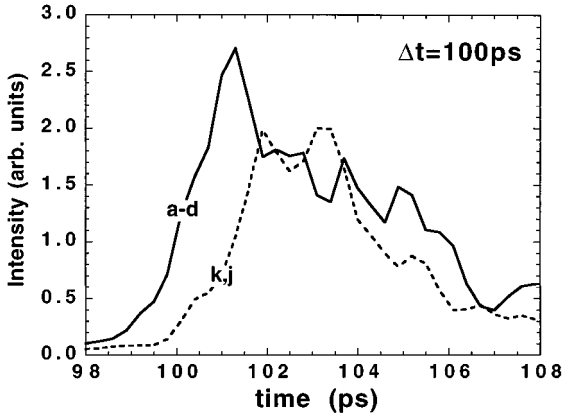

FIG. 15. Time history of Li-like $a-d$ and k,j satellite lines obtained during the interaction of a 10^{16}-W/cm^2 laser pulse with an aluminum plasma created 100 ps earlier by a similar pulse.

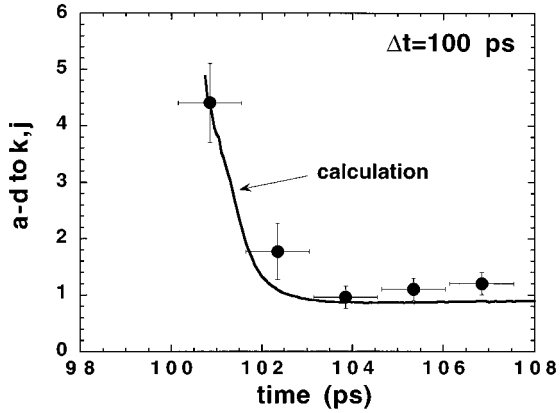

FIG. 16. Measured time history of Li-like $a-d$ to k,j ratio (dots) and comparison with calculation (line). The delay between both laser pulses is 100 ps.

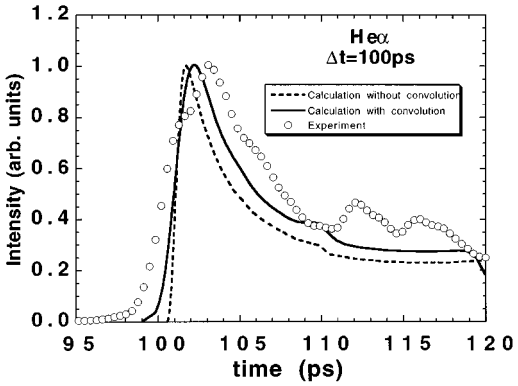

FIG. 17. Time history of the He_α line obtained with a 100-ps delay between both laser pulses. The dots represent the experimental result and the dotted line is the time history calculated with the hydrodynamics code coupled to TRANSPEC. This calculation was convolved with a 1.5-ps FWHM Gaussian to take account of the instrumental resolution (full line).

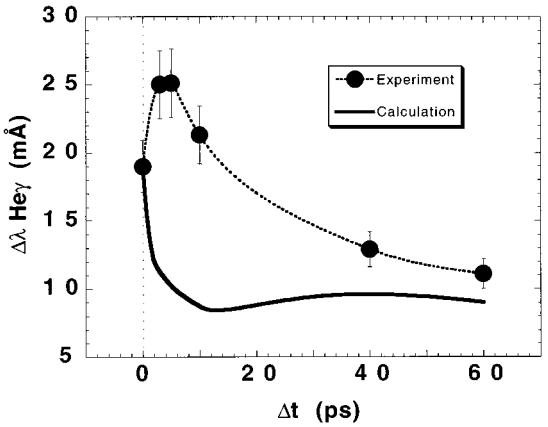

FIG. 18. Full width at half maximum of the time-integrated aluminum He_γ line obtain when the laser pulse interacts with a plasma created at certained time (Δt) earlier. Experimental data are represented by the dots and the full line indicates the results of the simulation.

lated integrated profile (Fig. 8) for the case of one pulse irradiation. As an ultimate benchmark test, we measured the He_γ time-integrated line profile as a function of the delay between both laser pulses. As shown in Fig. 18, an unexpected behavior is observed in these experiments. The He_γ width increases for small delays and presents a maximum for a delay of 5 ps. Calculations performed with $f=0.07$ (best agreement in the analysis of the Li-like satellite emission) as well as kinetic calculations (realized for a delay of 10 ps) do not reproduce the large width observed at small delays. It was recently proposed [46] that Li-like satellite emission, which is not included in our He_γ line profile calculation, could affect the shape of the He_γ line (mainly on its long-wavelength side), the effect being stronger for higher electron density. Our results seem to suggest that these satellites are enhanced in the nonlocal regime, thus strongly modifying the $1s4p$-$1s^2$ line profile. In the present experiment, this line is too weak to be time and/or space resolved. Further study is required to clarify the He_γ line profile behavior in the presence of strong non-Maxwellian effects.

VI. CONCLUSION

We used time-resolved spectroscopy to quantitatively understand the ionization and the plasma dynamics on the picosecond time scale. High-resolution spectroscopy of Li-like emission is used in the present work and gives us the possibility to study various regimes of ultrashort laser-matter interaction. Three different plasma regimes—the local thermal equilibrium regime, the transient nonlocal regime, and the transient Maxwellian regime—have been isolated and analyzed. Results obtained in those three regimes are compared to hydrodynamics calculations. Very good agreement is obtained when the laser pulse interacts either with an ultrashort density gradient scale length (LTE regime) or with a long gradient scale length (nonstationary Maxwellian regime). For the case of an interaction with an intermediate density gradient scale length, calculation results strongly depend on the way thermal transport is treated and thus the time history of the Li-like satellite lines is strongly affected by transient and nonlocal effects. These experiments allow us to benchmark calculations in the nonlocal regime.

ACKNOWLEDGMENTS

This work was supported in part by the Natural Sciences and Engineering Research Council of Canada, by the Fonds pour la Formation des Chercheurs et l'Aide à la Recherche, and by the Ministère de l'Éducation du Québec. The authors would like to thank J. P. Matte and S. Éthier for the FPI kinetic simulations, J. C. Gauthier and R. Marjoribanks for reviewing this work, and also Z. Jiang, J. F. Pelletier, H. Pépin, and M. Chaker for many fruitful discussions. The technical support from F. Poitras and C. Sirois is also acknowledged.

[1] H. M. Milchberg, R. R. Freeman, S. C. Davey, and R. M. More, Phys. Rev. Lett. **61**, 2364 (1988).
[2] M. Murnane, H. C. Kapteyn, and R. W. Falcone, Phys. Rev. Lett. **62**, 155 (1989).
[3] J. C. Kieffer, P. Audebert, M. Chaker, J. P. Matte, H. Pépin, T. W. Johnston, P. Maine, D. Meyerhofer, J. Delletrez, D. Strickland, P. Bado, and G. Mourou, Phys. Rev. Lett. **62**, 760 (1989).
[4] J. C. Kieffer, M. Chaker, J. P. Matte, H. Pépin, C. Y. Côté, Y. Beaudoin, T. W. Johnston, C. Y. Chien, S. Coe, G. Mourou, and O. Peyrusse, Phys. Fluids B **5**, 2676 (1993).
[5] B. Soom, H. Chen, Y. Fisher, and D. D. Meyerhofer, J. Appl. Phys. **74**, 5372 (1993).
[6] G. A. Kyrala, R. D. Fulton, E. K. Wahlin, L. A. Jones, G. T. Shappert, J. A. Cobble, and A. J. Taylor, Appl. Phys. Lett. **60**, 2195 (1992).
[7] P. Audebert, J. P. Geindre, J. C. Gauthier, A. Mysyrowicz, P. Chambaret, and A. Antonetti, Europhys. Lett. **19**, 189 (1992).
[8] J. D. Kmetec, C. L. Gordon III, J. J. Macklin, B. E. Lemoff, G. S. Brown, and S. E. Harris, Phys. Rev. Lett. **68**, 1527 (1992).
[9] J. A. Cobble, G. A. Kyrala, A. A. Hauer, A. J. Taylor, C. C. Gomez, N. D. Delamater, and G. J. Schappert, Phys. Rev. A **39**, 454 (1989).
[10] D. G. Stearns, O. Landen, E. M. Campbell, and J. H. Scofield, Phys. Rev. A **37**, 1684 (1988).
[11] O. Peyrusse, J. C. Kieffer, C. Y. Côté, and M. Chaker, J. Phys. B **26**, L511 (1993).
[12] R. C. Mancini, P. Audebert, J. P. Geindre, A. Rousse, F. Falliès, J. C. Gauthier, A. Mysyrowicz, J. P. Chambaret, and A. Antonetti, J. Phys. B **27**, 1671 (1994).
[13] J. P. Matte, J. C. Kieffer, S. Éthier, M. Chaker, and O. Peyrusse, Phys. Rev. Lett. **72**, 1208 (1994).
[14] J. C. Kieffer, M. Chaker, T. W. Johnston, C. Y. Chien, S. Coe, G. Mourou, and J. Dubau, Phys. Rev. Lett. **68**, 480 (1992).
[15] J. C. Kieffer, Y. Beaudoin, M. Chaker, C. Y. Côté, H. Pépin, C. Y. Chien, S. Coe, and G. Mourou, in *X-Ray Lasers 92*, Proceedings of the Third International Colloquium, edited by E. E. Fill, IOP Conf. Proc. No. 125 (Institute of Physics and

Physical Society, London, 1992); J. C. Kieffer, Y. Beaudoin, M. Chaker, C. Y. Côté, Z. Jiang, T. W. Johnston, J. P. Matte, C. Y. Chien, S. Coe, G. Mourou, O. Peyrusse, A. Mens, R. Verecchia, R. Sauneuf, D. Schirmann, and J. Dubau, in *OSA Proceedings on Short Wavelengths V*, edited by P. B. Corkum and M. D. Perry (Optical Society of America, Washington, D.C., 1993), Vol. 17, pp. 196–199.

[16] J. C. Kieffer, M. Chaker, J. P. Matte, C. Y. Côté, Y. Beaudoin, Z. Jiang, C. Y. Chien, S. Coe, G. Mourou, O. Peyrusse, and D. Gilles, SPIE Proc. **1860**, 127 (1993).

[17] J. C. Kieffer, Z. Jiang, A. Ikhlef, C. Y. Côté, and O. Peyrusse, J. Opt. Soc. Am. B **13**, 132 (1996).

[18] J. F. Pelletier, M. Chaker, and J. C. Kieffer, Opt. Lett. **21**, 1040 (1996).

[19] C. Rouyer, É. Mazataud, I. Allais, A. Pierre, S. Seznec, C. Sauteret, G. Mourou, and A. Migus, Opt. Lett. **18**, 214 (1993).

[20] R. Shepherd (private communication); R. Shepherd, R. Booth, D. Price, M. Bowers, D. Swan, J. Bonlie, B. Young, J. Dunn, B. White, and R. Stewart, Rev. Sci. Instrum. **66**, 719 (1995).

[21] J. Workman, A. Maksimchuk, X. Liu, U. Ellenberger, J. S. Coe, C. Y. Chien, and D. Umstadter, Phys. Rev. Lett. **75**, 2324 (1995).

[22] Z. Jiang, J. C. Kieffer, J. P. Matte, M. Chaker, O. Peyrusse, D. Gilles, G. Korn, A. Maksimchuk, S. Coe, and G. Mourou, Phys. Plasmas **2**, 1702 (1995).

[23] This code is briefly described in Ref. [42].

[24] D. R. Bates, F. R. S. Kingston, and R. W. P. McWhirter, Proc. R. Soc. London, Ser. A **267**, 297 (1962); **270**, 155 (1962).

[25] J. P. Raucourt and M. Busquet, J. Quant. Spectrosc. Radiat. Transf. **54**, 81 (1995).

[26] L. Spitzer, *Physics of Fully Ionized Plasmas* (Wiley Interscience, New York, 1962); L. Spitzer and R. Harm, Phys. Rev. **89**, 977 (1953).

[27] L. Schlessinger and J. Wright, Phys. Rev. A **20**, 1934 (1979).

[28] A. B. Langdon, Phys. Rev. Lett. **44**, 575 (1980).

[29] D. Vick, C. E. Capjack, and W. Rozmus, Comments Plasma Phys. Control. Fusion **17**, 87 (1996).

[30] W. L. Kruer, *The Physics of Laser Plasma Interactions* (Addison-Wesley, New York, 1988).

[31] E. M. Epperlein and R. W. Short, Phys. Fluids B **4**, 2211 (1992).

[32] J. J. Duderstadt and G. A. Moses, *Inertial Confinement Fusion* (Wiley, New York, 1982).

[33] Y. T. Lee and R. M. More, Phys. Fluids **27**, 1273 (1984).

[34] O. Peyrusse, Phys. Fluids B **4**, 2007 (1992).

[35] A. H. Gabriel and T. M. Paget, J. Phys. B **5**, 673 (1972).

[36] V. L. Jacobs and M. Blaha, Phys. Rev. A **21**, 525 (1980).

[37] A. Zigler, V. L. Jacobs, D. A. Newman, P. G. Burkhalter, D. J. Nagel, T. S. Luk, A. McPherson, K. Boyer, and C. K. Rhodes, Phys. Rev. A **45**, 1569 (1992).

[38] J. C. Kieffer, C. Y. Côté, Z. Jiang, Y. Beaudoin, M. Chaker, and O. Peyrusse, Can. J. Phys. **72**, 802 (1994).

[39] D. Strickland and G. Mourou, Opt. Commun. **56**, 219 (1985).

[40] Y. Beaudoin, C. Y. Chien, J. S. Coe, J. L. Tapié, and G. Mourou, Opt. Lett. **17**, 865 (1992).

[41] C. Y. Côté, Ph. D. thesis, INRS-Université du Québec, 1996 (unpublished); C. Y. Côté, Z. Jiang, J. C. Kieffer, A. Ikhlef, H. Pépin, and O. Peyrusse, in *Atomic Processes in Plasmas*, edited by A. Osterheld and W. Goldstein, Proceedings of the 10th APS Topical Meeting on Atomic Processes in Plasmas, AIP Conf. Proc. No. 381 (AIP, New York, 1996).

[42] J. C. Kieffer, M. Chaker, C. Y. Côté, Y. Beaudoin, H. Pépin, C. Y. Chien, S. Coe, and G. Mourou, Appl. Opt. **32**, 4247 (1993).

[43] O. Peyrusse, M. Busquet, J. C. Kieffer, Z. Jiang, and C. Y. Côté, Phys. Rev. Lett. **75**, 3862 (1995).

[44] S. Éthier, Ph. D. thesis, INRS-Université du Québec, 1996 (unpublished).

[45] J. P. Matte and J. Virmont, Phys. Rev. Lett. **49**, 1936 (1982); J. P. Matte, T. W. Johnston, J. Delletrez, and R. L. McCrory, *ibid.* **53**, 1461 (1984).

[46] R. C. Mancini, A. S. Shlyaptseva, and A. Antonetti, Phys. Rev. E **54**, 4147 (1996).